https://dx.doi.org/10.1016/j.compind.2023.104066

Process Parameter Effects Estimation and Surface Quality Prediction for Selective Laser Melting Empowered by Bayes Optimized Soft Attention Mechanism-Enhanced Transfer Learning

Jianjian Zhu [a,b,c,*], Zhongqing Su [b,c], Qingqing Wang [b,d], Runze Hao [e], Zifeng Lan [f], Frankie Siu-fai Chan [g], Jiaqiang Li [h], Sidney Wing-fai Wong [g]

[a] *College of Aviation Engineering, Civil Aviation Flight University of China, Guanghan 618311, P.R. China*

[b] *Department of Mechanical Engineering, The Hong Kong Polytechnic University, Kowloon, Hong Kong S.A.R.*

[c] *The Hong Kong Polytechnic University Shenzhen Research Institute, Shenzhen 518057, P.R. China*

[d] *School of System Design and Intelligent Manufacturing, Southern University of Science and Technology, Shenzhen 518055, P.R. China*

[e] *Hefei Zhongke Chongming Technology Co., Ltd, Hefei 230009, P.R. China*

[f] *School of Engineering, The University of Tokyo, Tokyo 113-8654, Japan*

[g] *Industrial Center, The Hong Kong Polytechnic University, Kowloon, Hong Kong S.A.R.*

[h] *School of Mechanical and Electric Engineering, Soochow University, Suzhou 215021, P.R. China*

[*] Corresponding author: Jianjian Zhu (Associate Professor, Postdoctoral Research Fellow, Ph.D.)

Email: zhujj.work@outlook.com

Abstract:

Additive manufacturing (AM), particularly selective laser melting (SLM), has revolutionized the industrial manufacturing sector owing to its remarkable design flexibility and precision. However, it is well known that slight changes in SLM process parameters may highly affect the surface quality of the as-built product. In this paper, we investigate the influence of SLM printing parameters (laser power, laser scanning speed, layer thickness, and hatch distance) on surface quality and develop a predictive model for surface quality based on the given printing parameters. The developed model is constructed by a Bayesian Optimization and soft Attention mechanism-enhanced Transfer learning (BOAT) framework with superior domain adaptability and generalization capability. Through experimental validation, the effectiveness of the BOAT approach in estimating printing parameters and correlating them with surface quality has been verified. The comprehensive methodology, experimental configurations, prediction results, and ensuing discussions are all presented. This study contributes to providing valuable insights and practical implications for improving the competitiveness and impact of SLM in advanced manufacturing by accurately predicting surface quality with specified printing parameters.

Keywords:

Additive manufacturing; Selective laser melting; Bayesian optimization; Transfer learning; Attention mechanism

1. Introduction

Additive manufacturing (AM), also known as 3D printing, has gained widespread usage in industrial manufacturing due to its exceptional design flexibility and high precision in fabricating intricate and customized components. Selective laser melting (SLM), increasingly referred to as laser powder bed fusion (LPBF) in AM community, is a notable metal AM process that has emerged as a revolutionary technique in advanced manufacturing. Similar to the conventional machining processes, SLM's high surface quality is a basic feature, which is a critical aspect that significantly influences the overall performance and integrity of the produced parts [1]. Inadequate surface quality may result in the formation of defects such as cracks, porosity, and substandard roughness, compromising the functionality of manufactured parts [2]. Additionally, the utilization of SLM in various industries is hindered by its high cost, encompassing expenditures on equipment, materials, and labor. Currently, optimizing printing parameters for SLM is a complex and time-consuming process due to the involvement of multiple variables. The lack of a streamlined approach further exacerbates the costs and time requirements associated with SLM. Therefore, it is crucial to identify the impacts of printing parameters on surface quality and develop novel approaches to enhance the competitiveness of SLM and its impact on the manufacturing industry.

Researchers and industry professionals have made significant efforts over the past decades to improve the surface quality of SLM-formed parts. It was found that the surface quality strongly depends on the powder (e.g., grain size [3], morphology [4],

chemical composition [5]). Sendino et al. [3] investigated the effects of Particle Size Distribution (PSD) on surface finish of SLM-formed parts by printing with Inconel 718 powders of varying PSD. Their study suggests a strong correlation between surface roughness and the fraction of smaller particles within the PSD of the batch. However, no relationship was found between surface roughness and the larger particles. The morphology of the powder particles also influences surface finish, with fewer spherical particles contributing to higher surface roughness [4]. In the study conducted by Miao et al [5], who utilized a mixture of powders (AlSi10Mg-316L) for SLM fabrication, their findings suggest that powder composition has a notable impact on surface roughness. The overall mean roughness decreases with an increase in AlSi10Mg content. This phenomenon was attributed to the superior wettability of AlSi10Mg compared to 316L and the smaller average particle size of AlSi10Mg in comparison to the 316L powder.

More studies have concentrated on examining the impact of various process parameters on surface quality in SLM. Numerous experimental investigations have explored the influence of different parameters, including laser power [6–10], scanning speed [7–10], layer thickness [6], hatch spacing [6,8,9], scanning strategy [11], inclination angle [10], exposure time [6]. Additionally, some investigations have gained insights into the effects of process parameters on surface quality using physics-driven methods. Khorasani et al. [12] mathematically characterized the thermal effects of process parameters on the average surface of SLM Ti6Al4V samples. Their results

indicated that higher energy density and temperature result in lower surface tension and capillary force, leading to unstable and lower surface quality. However, due to the multitude of influential parameters and the complexity of their potential interactions, the aforementioned studies have typically focused on only a subset of parameters at a time. Moreover, both experimental works and physics-based modeling are generally expensive and time-consuming, making it nearly impossible to conduct them simultaneously in large quantities.

Hence, there is a significant interest in developing optimization algorithms for SLM parameters based on multidimensional datasets. Various approaches for optimizing process parameters exist, such as the Taguchi method [13,14], Response Surface Method (RSM) [15,16], and genetic algorithms [17,18]. Li et al. [16] proposed an RSM-based method to enhance the surface quality of SLM-formed Ti6Al4V parts, investigating the relationship between SLM process parameters (power, scanning speed, and scanning space) and surface roughness. They obtained optimal process parameters using the RSM method, which were experimentally verified. Xia et al. [18] utilized a multi-objective genetic algorithm to create a predictive model of surface quality involving four key process parameters (defocusing amount, laser power, scan speed, and layer thickness). The obtained model was then employed to optimize the process parameter combination, enhancing the surface quality of SLM-formed parts. However, these optimization algorithms were typically employed to investigate only specific parameters, limiting their ability to generalize SLM characteristics.

In addition to the aforementioned approaches, data-driven Machine Learning (ML) is an approach that can simplify the process of finding suitable SLM parameters and avoid the high costs associated with experiments and testing. This approach has been widely used in the AM community [19–24]. Some studies in this domain have focused on process parameter optimization [5,25], defect prediction [26,27], and surface quality prediction [28]. Supervised learning models in ML can be considered as black-box functions [29] and can be directly integrated into a parameter optimization workflow. In short, these functions take the process parameters of printing (e.g., laser power, scanning speed, layer thickness, hatch distance) as input variables, and the output could be relative density, surface roughness, hardness, and mechanical properties. Nguyen et al. [30] developed a supervised Artificial Neural Network (ANN) to optimize the relative density of a product manufactured by SLM. Chen et al. [31] developed a supervised gradient descent-based neural network model to detect track defects and identify suitable parameter combinations (i.e., laser power and scanning velocity) to fabricate defect-free tracks. Bao et al. [32] developed a Support Vector Machine (SVM) model for predicting the fatigue life of SLM Ti6Al4V samples. The results indicate that the developed model has higher accuracy in prediction than another ML method, i.e., the k-nearest neighbor algorithm. Other ML models, such as Gaussian Process Regression (GPR) [33,34], Random Forest Regression (RFR) [35,36], and Adaptive Neuro-Fuzzy Inference System (ANFIS) [28,37], also find applications in SLM. La Fé-Perdomo et al. [38] conducted a comprehensive comparison study of statistical (RSM)

and ML-based approaches (ANN, SVM, GPR, RFR, and ANFIS) for modeling the relationship between four process parameters (laser power, scanning speed, hatch distance, and layer thickness) and surface roughness, relative density, and mechanical properties of 316L stainless steel specimens. Their investigation shows that it is impossible to accurately predict all the studied variables using a single model, and more than one technique is necessary for reliable forecasting.

However, ML models for SLM applications still have certain limitations despite their effectiveness. Some studies focused on specific materials or applications, which limits their generalizability [39,40]. Others that considered only a short range of process parameters may not provide a comprehensive understanding of their effects on printed parts. Conversely, when the range of process parameters increases, resulting in large amounts of labeled data, the computational resources and time consumption for training ML models from scratch could significantly increase. Furthermore, the high cost of raw materials for metal additive manufacturing is often not taken into account, and many studies do not consider the economic feasibility or practicality of implementing proposed process parameters in real-world manufacturing settings. Hence, it is often costly to obtain a satisfying model of high performance.

A promising approach, named transfer learning (TL), can overcome these drawbacks. TL can leverage the prediction ability of a previously trained model, requiring much less training data and reducing time and cost for constructing a new model for a targeted task. Moreover, TL can bridge among various data sources that

reveal common information of interest [41]. The pre-trained model could serve as a general model used as a feature extractor for a new classifier. For example, Li et al. [42] utilized the well-known deep VGG16 model as a pre-trained model, initially trained on an AM-unrelated dataset (i.e., ImageNet) to extract intrinsic and common features from raw image data. A TL model is further constructed with fine-tuning for in-situ quality inspection of SLM products. Similar TL models in AM can be found in some other references [43–45]. Also, the pre-trained model could be acquired from a related domain to improve performance in a target domain. The transfer directions of applying such models include TL across different AM processes (e.g., from LPBF to binder jetting [46], from bead-on-plate process to bead-on-powder process in LPBF [47]), different materials (e.g., from 316L stainless steel to CuSn8 bronze [48], from Ti6Al4V to 316L stainless steel [49]), different printers [50,51], and various geometries of AM products [52,53].

Inspired by the successful applications of TL in AM and to overcome the limitations of conventional ML approaches, we develop an ensemble approach called BOAT (Bayesian Optimization and soft Attention mechanism-enhanced Transfer learning) for surface quality prediction of SLM. The proposed BOAT approach offers prominent generalization capabilities, feature identification, prediction accuracy on small datasets based on previous data, and low training costs. To demonstrate the efficiency of BOAT, experiments were conducted on sample fabrication using Fused Deposition Modeling (FDM) and SLM processes. The resulting data was used to

construct datasets for validation. In the developed model, knowledge learned from the FDM dataset was transferred to the SLM dataset to construct the BOAT model. The hypothesis that the FDM-printed samples can help with the training TL model used in the scenario of SLM is based on the facts that SLM and FDM both have some underlying similarities: both FDM and SLM employ a layer-by-layer approach to fabricate objects, and they progressively melt and stack materials at each level, ultimately forming the desired object. The experimental validation results were analyzed using four performance indicators: Accuracy, Precision, Recall, and F1-score. Additionally, training history plots and Confusion Matrix (CM) diagrams were used to visually compare different hyperparameters at various magnitudes.

Overall, we have demonstrated the effectiveness of the proposed BOAT approach for estimating the correlation between printing parameters and surface quality (represented by surface roughness in this study) on a small dataset involving SLM-printed samples using data obtained from similar issues. The subsequent sections of this paper will present the methodology, experimental configurations, results, and delve into the research findings to discuss their implications in further detail.

2. Selective laser melting process and fundamentals of BOAT approach

2.1. Description of selective laser melting

SLM is a sophisticated AM process that utilizes a high-power laser to selectively merge metallic powders, forming intricate three-dimensional structures layer by layer.

This technique provides precise management over the melting dynamics, allowing for the fabrication of highly personalized components boasting exceptional mechanical and geometric properties [54]. **Fig. 1** displays a schematic illustration of the SLM process, delineating the key components integral to an SLM printing facility [7,11,55].

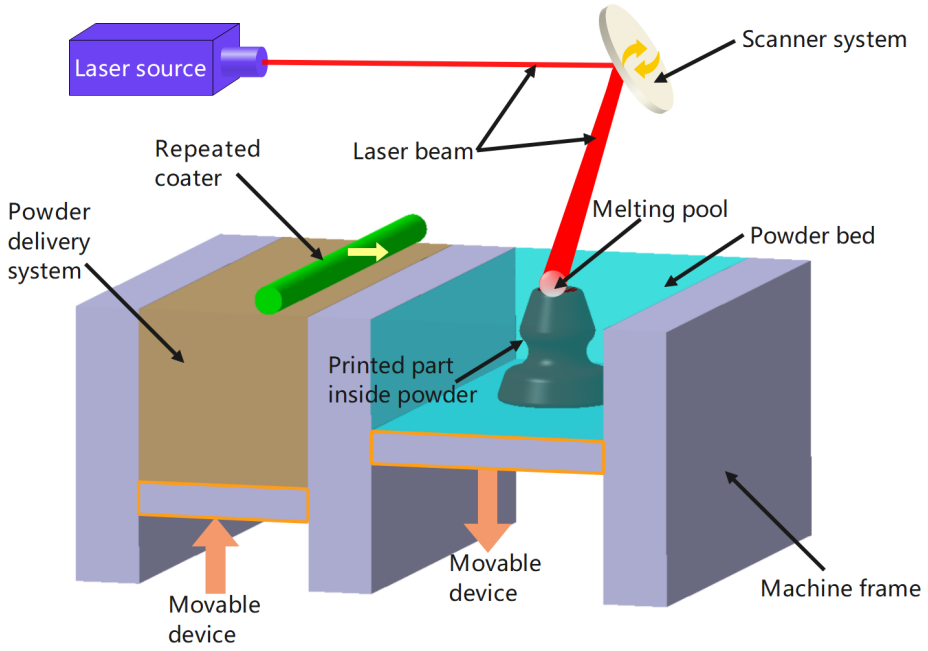

Fig. 1. Schematic illustration of the SLM printing process.

The SLM process initiates with the conversion of a computer-aided design (CAD) model into discrete horizontal layers. Following this, a uniform layer of powdered material (e.g., titanium, steel, nickel, alloys, ceramics, composites [54]) is evenly spread onto a build platform. By precisely scanning a focused laser beam, each layer undergoes selective melting, conforming to the desired design specifications. The ultimate quality of SLM parts is influenced by numerous process parameters (powder-related, laser-related, and powder-bed-related variables [56]), owing to the intricate system and

mechanisms involved.

SLM using Ti6Al4V powder is a widely studied topic by researchers from diverse fields. Despite encountering challenges, such as the formation of defects during the SLM process, researchers persist in improving and optimizing fabrication parameters. Their goal is to maximize the utilization of Ti6Al4V material through the SLM technique by precisely controlling laser parameters and powder bed characteristics. It is possible to achieve high-density parts with favorable mechanical and metallurgical properties. This technique finds profound utility across diverse industries such as aerospace, automotive, and biomedical, where the demand for tailor-made and high-performance parts remains paramount [57,58].

2.2. Fundamental of the BOAT approach

In present-day practice, the correlation between process parameters and surface quality of the part fabricated by SLM is predominantly established through iterative experimentation, also known as trial-and-error. However, the trial-and-error approach has significant drawbacks, including being time-consuming, lacking systematicity, relying on subjective judgment, and being sensitive to initial conditions and environmental factors. Therefore, there is an urgent need to develop novel approaches to address these limitations and provide efficient and reliable parameter optimization strategies [10]. This necessity has motivated the proposal of the BOAT approach mentioned in this section, which aims to overcome the shortcomings of the currently

employed method by implementing a more systematic and objective optimization strategy [59,60].

2.2.1. Soft attention mechanism-enhanced 1DCNNs

In recent years, the attention mechanism has played a significant role in enhancing the performance of intelligent models by enabling them to focus on relevant information selectively. These mechanisms provide a foundation for developing more sophisticated models with an improved understanding of complex data patterns. The attention mechanism operates by assigning weights to different elements of the input sequence or feature map, emphasizing more relevant information and suppressing less important ones.

Over the past decades, One Dimensional Convolutional Neural Networks (1DCNNs) have been extensively employed in sequence data processing. However, the conventional 1DCNNs may not effectively identify and highlight important features in complex input data, generally in a sequence. To overcome this obstacle, the attention mechanism is employed to enhance the capability of attention-based convolutional neural networks to capture significant feature dependencies at various scales. This is achieved by focusing on different parts of the input sequence [61,62].

Supposing there is an input sequence $\boldsymbol{X}$, which can be expressed by Eq. (1):

$$\boldsymbol{X} = [\boldsymbol{x}_1, \boldsymbol{x}_2, \cdots, \boldsymbol{x}_N] \in \mathbb{R}^{D \times N} \tag{1}$$

where $\boldsymbol{x}_n$ is a vector with n dimensions ($n \in [1, N]$), and $\boldsymbol{x}_n \in \mathbb{R}^{D}$. The soft attention

mechanism is deployed in this study. Given a task-related query vector $\boldsymbol{q}$, we use the attention variable $z \in [1, N]$ to denote the index position of the selected information. Specifically, $z = n$ indicates that the n-th input vector has been chosen. The probability α_n of selecting the n-th input vector, given $\boldsymbol{q}$ and $\boldsymbol{X}$, can be computed using the following Eq. (2):

$$\begin{aligned} \alpha_n &= P\left(z = n \middle| \boldsymbol{X}, \boldsymbol{q}\right) \\ &= soft\max\left(s\left(\boldsymbol{x}_n, \boldsymbol{q}\right)\right) \\ &= \frac{e^{s\left(\boldsymbol{x}_n, \boldsymbol{q}\right)}}{\sum_{j=1}^{N} e^{s\left(\boldsymbol{x}_j, \boldsymbol{q}\right)}} \end{aligned} \tag{2}$$

where α_n is referred to as the attention distribution, and $s(\boldsymbol{x}, \boldsymbol{q})$ represents the attention scoring function. In this study, the scoring function is a dot production given by Eq. (3):

$$s\left(\boldsymbol{x}, \boldsymbol{q}\right) = \boldsymbol{x}^T \boldsymbol{q} \tag{3}$$

Then the attention can be calculated by the following Eq. (4):

$$att\left(\boldsymbol{X}, \boldsymbol{q}\right) = \sum_{n=1}^{N} a_n \boldsymbol{x}_n = \mathrm{E}_{z:\ p\left(z|X, \boldsymbol{q}\right)}\left[\boldsymbol{x}_z\right] \tag{4}$$

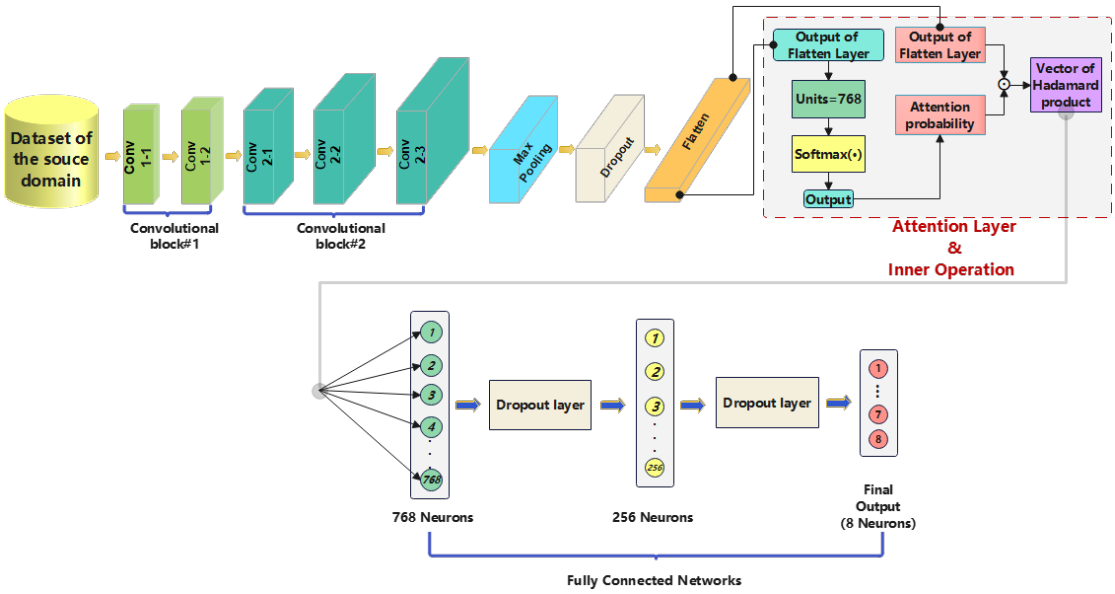

Fig. 2. Customized architecture of the soft attention mechanism-enhanced 1DCNNs.

Particularly, the customized architecture and operating principle of the proposed Attention mechanism-enhanced CNNs (ACNNs) with one-dimension can be diagrammatically illustrated in **Fig. 2**. This figure illustrates the architecture of the model, which comprises an input layer, two convolutional blocks for feature extraction from the provided dataset, and additional layers for dimension reduction, preventing overfitting, and transforming multidimensional data into a one-dimensional form. Additionally, a customized architecture includes an attention layer with an inner operation that highlights the most important information transmitted from the preceding layers. The data processed by the attention layer is subsequently inputted into a classifier consisting of fully connected networks.

The ACNNs model depicted in **Fig. 2** aims to achieve a high-performance pre-trained base model (PBM) that will be used in the proposed BOAT approach. The

ultimate output of the ACNNs model is the classification of the dataset in the source domain into different classes based on surface roughness magnitudes. Furthermore, the hyperparameters of the ACNNs model are optimized using the Bayesian algorithm to obtain the optimal combinations and the best-performing model.

2.2.2. Fundamentals of the proposed BOAT approach

The proposed BOAT approach incorporates well-known Bayesian optimization algorithms, a customized ACNN architecture described in the previous section, and a fine-tuning-based TL strategy. Fine-tuning is a widely used technique in the TL community, involving training a pre-trained model on a large dataset and then adapting it to a new task with a limited amount of labeled data [63,64]. The fine-tuning process starts by initializing the model parameters with the pre-trained model, which has typically been trained on a related task or dataset. The initialized parameters are then further refined through additional training on the target task. This approach allows the model to leverage the generic features and representations learned from the PBM, thus speeding up the learning process for the specific target task [65].

In the TL community, it is customary to freeze the lower layers of the pre-trained model during fine-tuning. These lower layers typically consist of convolutional layers that are responsible for capturing low-level features. Meanwhile, only the higher layers, such as fully connected layers that are more task-specific, are updated during the fine-tuning process. By employing this selective fine-tuning strategy, the model preserves

the generic features learned by the lower layers while enabling the higher layers to adjust and specialize for the nuances of the target task.

Generally, the objective of fine-tuning is captured by the objective expression given in Eq. (5):

$$L_{\text{tuning}} = \alpha \cdot L_{\text{source}} + \beta \cdot L_{\text{target}} \tag{5}$$

where α and β are weighting parameters that balance the influence of the source task loss L_{source} and the target task loss L_{target}. The model parameter update rule during fine-tuning is represented as the equation below:

$$\theta_{\text{new}} = \theta_{\text{old}} - \lambda \cdot \frac{\partial L_{\text{tuning}}}{\partial \theta} \tag{6}$$

where θ_{new} and θ_{old} denote the updated and current model parameters, respectively. λ is the learning rate and $\partial L_{\text{tuning}} / \partial \theta$ indicates the gradient of the objective function concerning the model parameters.

Furthermore, considering a source task T_s and a target task T_t, with input spaces χ_s and χ_t, alongside output spaces γ_s and γ_t respectively, the goal of fine-tuning is to improve the performance of the target task T_t. Features $f_{\theta_s}(\cdot)$ can be obtained on a source task T_s from a pre-trained model. Then, it can be fine-tuned with a model $h_{\theta_t}(\cdot)$ for predicting target tasks T_t alongside a loss function $L_T(h_{\theta_t})$. Therefore, the problem for fine-tuning TL can be yielded as the below Eq. (7):

$$\min_{\theta_t} L_T(h_{\theta_t}) = \sum_{x_i \in D_t} l(h_{\theta_t}(f_{\theta_s}(x_i)), y_i) \tag{7}$$

where $l(\cdot,\cdot)$ is the loss function and y_i is the true label of x_i. By optimizing Eq. (7), a model with better performance on the target task can be obtained. Overall, the use of

fine-tuning allows for the effective adaptation of pre-trained models to new tasks, even when there is limited labeled data available. This approach facilitates the development of task-specific models in resource-constrained scenarios, where training a model from scratch might be impractical or infeasible due to the scarcity of labeled data. Fine-tuning leverages the knowledge and representations learned by the pre-trained model, significantly reducing the amount of data required to achieve good performance on the target task. Thus, it offers an efficient solution for building task-specific models in resource-limited settings.

Regarding this study, the fine-tuning-based TL strategy utilizes ACNNs to transfer knowledge from the source domain to the target domain. This process is visually represented in **Fig. 3**, where the graphical illustration demonstrates how ACNNs are employed to transfer learned features and weights from the pre-trained model in the source domain to the target domain. By fine-tuning the transferred model using the data from the target domain, the ACNNs can adapt and generalize effectively to new tasks and datasets.

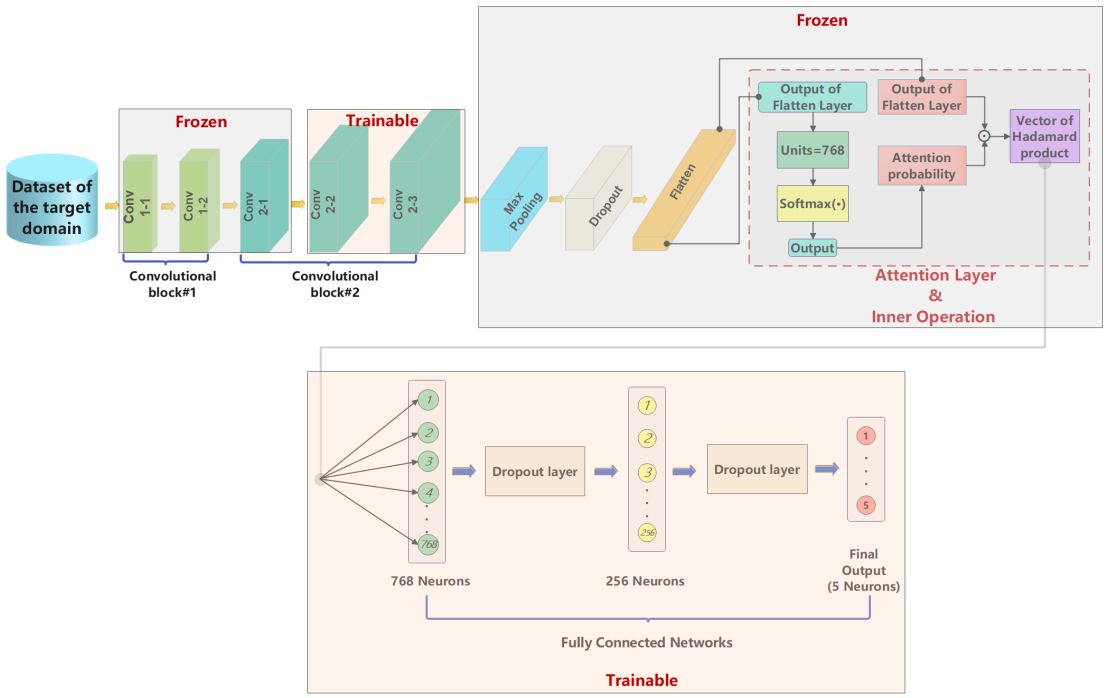

Fig. 3. Architecture of the fine-tuned ACNNs with frozen and trainable layers.

3. Experimental set-up and dataset construction

3.1. Experimental set-up

To validate the effectiveness of the proposed BOAT approach, we conducted two independent experiments using both FDM and SLM processes. Each experiment involved different printing parameters and specifications, allowing us to assess the performance of the BOAT approach in diverse printing scenarios. The primary objective of these experiments is to evaluate the efficacy of the BOAT, generalization capability, and accuracy across various applications, thus providing comprehensive evidence of its effectiveness.

In this study, the 3D-printed samples produced by the FDM process were considered the source domain, while the samples fabricated by SLM were categorized

as the target domain. Furthermore, the surface quality of these samples was characterized by measuring the surface quality using a laser microscope (VK-X200, Keyence Co. Ltd.). The material for FDM printing is Poly Lactic Acid (PLA) filament with a diameter of 1.75 mm, and for SLM printing is Ti6Al4V with a particle size generally ranging from 15 μm to 60 μm. The parameters relevant to the FDM and SLM printing process are enumerated in **Table 1**. Moreover, the values of FDM and SLM printing parameters are presented in **Table 2** and **Table 3**, respectively.

Table 1

Overall comparison between the source domain and target domain.

	Printing process	Sample sizes (Unit: mm)	Material	Sample quantity	Printing parameters (Input/Features)	Variable (Label)
Source domain	FDM	20×15×5	PLA filament	625	Material flow Scan speed Layer height Nozzle temp.	Surface roughness
Target domain	SLM	8×8×10	Ti6Al4V powder	79	Laser power Scan speed Layer height Hatch distance	

Table 2

Printing parameters of the FDM process used in experiments.

Layer height (mm)	Scan speed (mm/s)	Nozzle temperature (℃)	Material flow (%)
0.05	60	195	95
0.10	65	200	100
0.15	70	205	105
0.20	75	210	110
0.25	80	215	115

Table 3

Printing parameters of the SLM process used in experiments.

Laser power (W)	Scan speed (mm/s)	Hatch distance (mm)	Layer thickness (mm)
150	600	0.08	0.03
200	800	0.1	0.04
250	1000	0.12	0.05
300	1200	0.14	0.06

The fabricated samples, which were produced using the designed printing parameters and the FDM and SLM facilities, are depicted separately in **Fig. 4** and **Fig. 5**. The surface structure images of FDM and SLM-printed samples measured by the laser microscope are illustrated in **Fig. 6** and **Fig. 7**, demonstrating that the surface condition has no evident manufacturing defects. Besides, **Fig. 6** and **Fig. 7** illustrate the

different surface quality between FDM and SLM printing processes. By comparing **Fig. 6** and **Fig. 7**, it can be observed that the surface of the FDM printing is formed line by line, and the SLM is by layer-wise melting. However, we can also find numerous unmelted particles in **Fig. 7** (a), which significantly influence the quality of the initial surface. It should also be noted that only the exemplary samples are presented due to the difficulty of showing all the images in one paper.

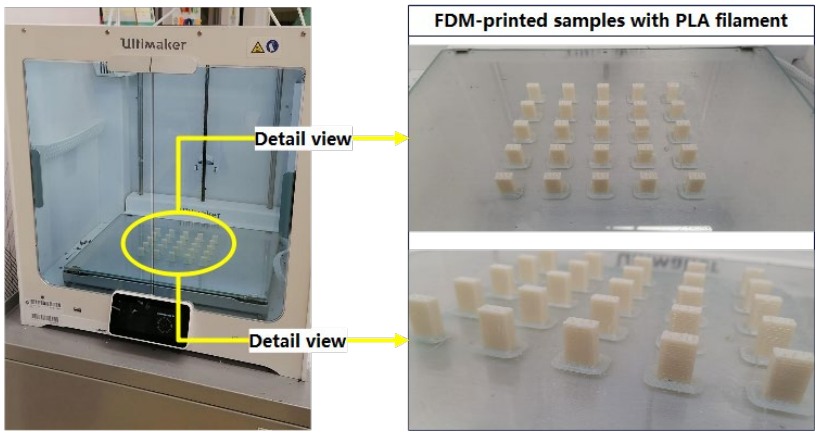

Fig. 4. FDM printing system used in experiments.

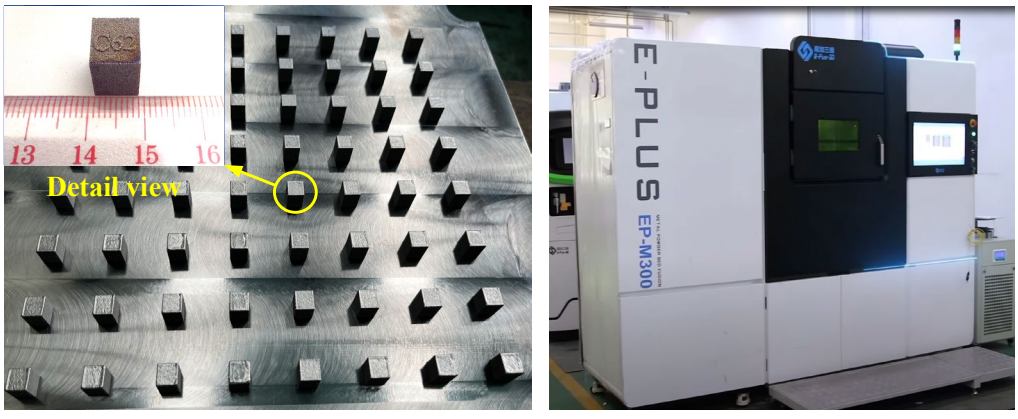

(a) **(b)**

Fig. 5. SLM printing system used in experiments: (a) fabricated titanium alloy samples, (b) EP-M300 SLM facility.

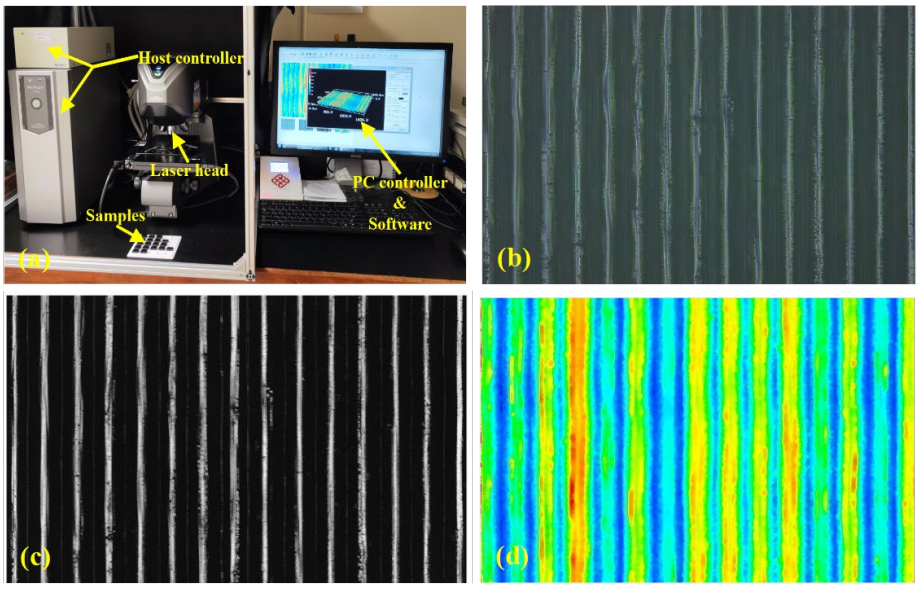

Fig. 6. Surface measurement of FDM-printed sample: (a) laser microscope system, (b) optical inspection image, (c) laser inspection image, (d) height map.

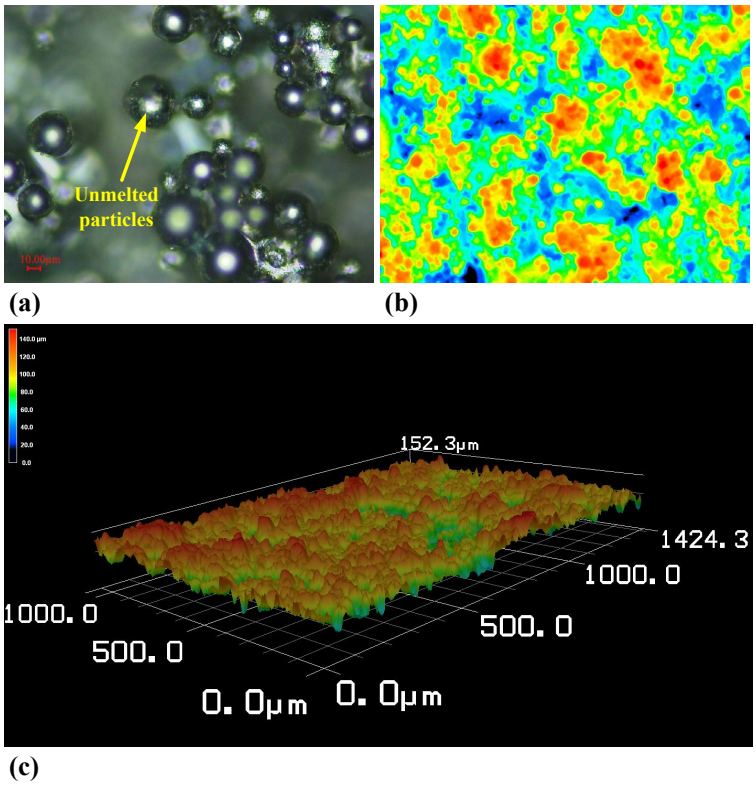

Fig. 7. Surface measurement of SLM-printed sample: (a) optical inspection image, (b) height map, (c) 3D surface microstructure.

3.2. Datasets construction using 3D-printed samples

Following the completion of an exhaustive assessment of the surface quality exhibited by the 3D-printed specimens, it becomes a viable prospect to compile and establish an inclusive dataset meticulously. The dataset from the source domain includes surface roughness data of FDM-printed samples with 625 entries, while the surface roughness data of the SLM-printed samples, comprising 79 entries, forms the target domain. The distribution of the surface roughness varying with the printing parameters has been illustrated in **Fig. 8**. **Fig. 8** (a) depicts the distribution of 625 data points of the FDM-printed samples based on surface roughness in a gradient manner, whereas **Fig. 8** (b) illustrates the distribution of the 79 SLM-printed samples according to surface roughness. The color bars on the right side of **Fig. 8** clarify the range of surface roughness in terms of the corresponding color.

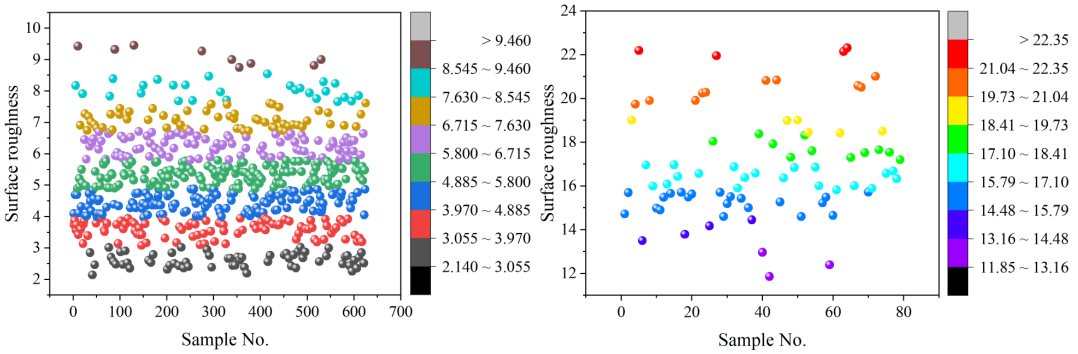

Fig. 8. Surface roughness distribution of 3D-printed samples: (a) data of FDM-printed samples in the source domain, (b) data of SLM-printed samples in the target domain.

By leveraging the data points depicted in **Fig. 8**, the dataset used for validating the proposed BOAT approach can be formulated. This dataset comprises four distinct features or dimensions, each accompanied by their corresponding labels. The independently constructed datasets for both the source and target domains are meticulously enumerated in **Table 4**, which exhibits that the printing parameters between the source and target domains have essential differences. **Table 4** has the four input features from Feat.1 to Feat.4 in the FDM and SLM printing scenarios, and each feature represents a kind of printing parameter. In this study, eighty percent of the data are used for training and the rest for model performance testing in the source and target domains. The built dataset aims to evaluate the surface quality of SLM printing based on other 3D printing processes with lower costs.

Furthermore, it is essential to note that the two datasets used in this study are independently categorized into eight and five classes regarding the surface roughness values. Each category represents a specific range of surface roughness, and the specific details of each surface roughness scope are enumerated in **Table 5**. This categorization provides a structured representation of the varying levels of surface roughness present in the datasets, allowing for a more comprehensive analysis and evaluation of the model's performance.

Table 4

Datasets in the source and target domains built with the initially experimental data.

Domains	Feat.1	Feat.2	Feat.3	Feat.4	Label	Category
Source domain (625 data)	Layer height (mm)	Scan speed (mm/s)	Nozzle temperature (℃)	Material flow (%)	Surface roughness (μm)	C1 to C8
	0.05	60	195	95	4.10	
	0.10	60	195	95	3.74	
	0.15	60	195	95	3.88	
	0.20	60	195	95	4.70	
	…	…	…	…	…	
	0.20	80	215	115	4.87	
	0.25	80	215	115	7.61	
Target domain (79 data)	Laser power (W)	Scan speed (mm/s)	Hatch distance (mm)	Layer thickness (mm)	Surface roughness (μm)	C1 to C5
	150	600	0.08	0.03	14.72	
	200	600	0.08	0.03	15.69	
	250	600	0.08	0.03	19.01	
	300	600	0.08	0.03	19.74	
	…	…	…	…	…	
	250	600	0.10	0.06	16.34	
	300	600	0.10	0.06	17.20	

Table 5

Categories and the corresponding surface roughness scope.

Categories	FDM-printed samples Source domain (Unit: μm)	SLM-printed samples Target domain (Unit: μm)
C1	Ra∈[2.0, 3.0)	Ra∈[11.5, 13.5)
C2	Ra∈[3.0, 4.0)	Ra∈[13.5, 15.5)
C3	Ra∈[4.0, 5.0)	Ra∈[15.5, 17.5)
C4	Ra∈[5.0, 6.0)	Ra∈[17.5, 19.5)
C5	Ra∈[6.0, 7.0)	Ra>19.5
C6	Ra∈[7.0, 8.0)	—
C7	Ra∈[8.0, 9.0)	—
C8	Ra∈[9.0, 10.0]	—

4. Results and discussion

4.1. Data pre-analysis and effects of printing parameters on surface roughness

This section presents a preliminary data analysis aimed at revealing the relationship between printing parameters and surface roughness, with the purpose of providing initial insights into the impact of these parameters on surface roughness. The analysis commenced by examining a diverse range of commonly manipulated printing parameters enumerated in **Table 2** and **Table 3**, respectively.

To capture practical variations encountered in real-world applications, different

levels were specifically chosen for each parameter. Subsequently, a series of test prints were generated under operational conditions using a standardized printing configuration. Surface roughness measurements were acquired in the laboratory. A three-dimensional scatter illustration has been depicted in **Fig. 9** based on the principle of controlling variates. It should be noted that the original set comprised 20 images with the dimension of four rows and five columns; however, to accommodate space constraints, only a subset of 4 exemplary images is presented herein. Above all, the original data obtained from the experiments were rigorously cleaned and preprocessed to ensure accuracy and reliability. There are 125 data points in each subplot of **Fig. 9** under the condition of keeping one of the printing parameters constant. The different colors are related to the magnitude of the surface roughness, which is clarified via a color bar on the right side. Similar to **Fig. 9**, the relationship between the printing parameters of the SLM process and the surface quality is also illustrated in **Fig. 10**.

Fig. 11 quantitatively depicts the estimation results of 3D printing parameters on the surface quality with bar graphs by calculating the feature importance scores with Decision Trees (DT)-based ensemble learning. **Fig. 11** (a) illustrates the 3D printing process of FDM, while **Fig. 11** (b) portrays the SLM 3D printing process. **Fig. 11** (a) shows that the printing parameter with the maximum effects on the FDM-printed 625 samples is layer height, while the printing parameter with the minimum effects is the scan speed. **Fig. 11** (b) indicates that the laser power has the largest impact on the surface roughness. The parameter that ranks second in terms of its impact on surface

quality is scan speed. Contrarily, the printing parameter that has the least impact on the surface quality of SLM-printed specimens is hatch distance. Particularly, it should be noted that the laser power and scan speed both have a combined effect on the heat input of the melt pool.

By closely examining the graphical representations, valuable insights can be gained regarding the distinctive impact of various printing parameters on surface quality within the context of FDM and SLM processes. Researchers and practitioners can utilize this information to comprehend the unique characteristics and limitations of these methods in achieving optimal surface quality. Furthermore, comprehensive analysis provided by **Fig. 11** offers valuable contributions to the advancement and optimization of 3D printing technology. It enhances comprehension regarding the intricate relationship between 3D printing parameters and surface quality across different processes, thereby facilitating further development in the field.

According to **Fig. 9** - **Fig. 11**, on the one hand, the data quantity can be intuitively compared between the source and target domains, composed of FDM-printed and SLM-printed samples, respectively. On the other hand, the complicated relationship between the surface quality and the printing parameters can be demonstrated, which indicates that it is quite challenging to be elucidated with a simple regression or other statistical methods. Through systematic manipulation of the printing parameters and measurement of the corresponding surface roughness, a comprehensive dataset was compiled, serving as a foundation for the proposed BOAT approach.

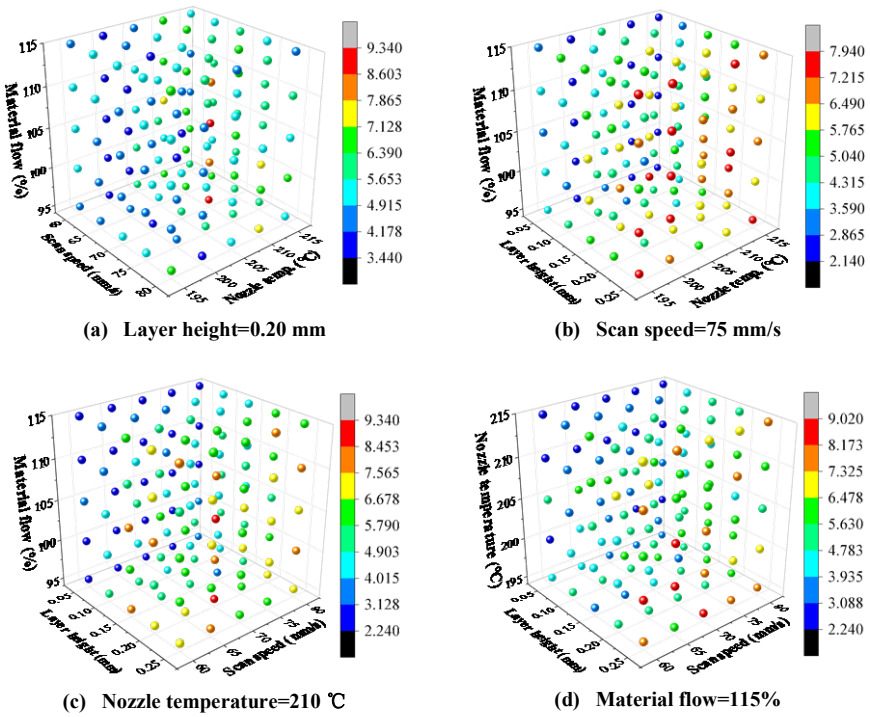

Fig. 9. Schematic of 3D scatter of the FDM-printed samples: (a) fixed layer height, (b) fixed scan speed, (c) fixed nozzle temperature, (d) fixed material flow.

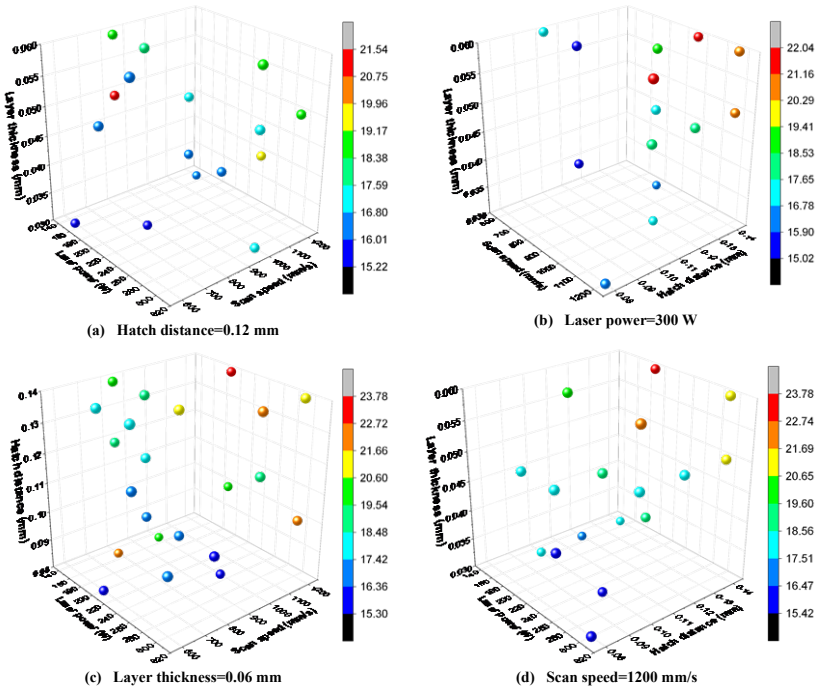

Fig. 10. Schematic of 3D scatter of the SLM-printed samples: (a) fixed hatch distance, (b) fixed laser power, (c) fixed layer thickness, (d) fixed scan speed.

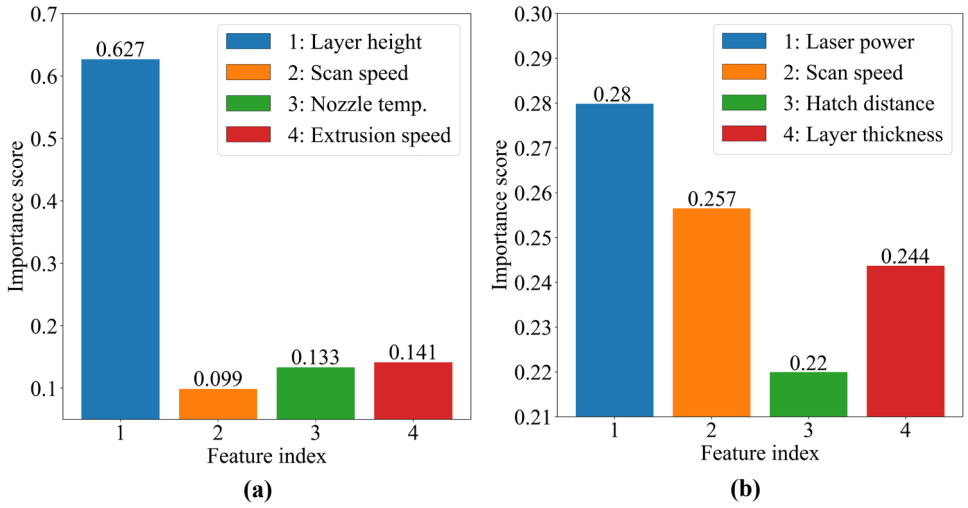

Fig. 11. Estimation of process parameter effects on surface quality by feature importance score: (a) FDM for source domain, (b) SLM for target domain.

4.2. Impact of hyperparameters on the PBM in the source domain

The PBM, which in this study is the ACNNs model, serves as the foundation of the proposed BOAT approach. It is important to highlight that the effectiveness of the PBM has a direct impact on the overall performance of the BOAT approach, particularly in terms of its ability to accurately predict surface roughness in various application scenarios. In this section, the relationship between the hyperparameters and the performance of the PBM is thoroughly examined. To achieve this, comparative analyses are carried out using a dataset comprising surface roughness data derived from samples produced through FDM-based 3D printing. These analyses provide insights into how different hyperparameter settings can influence the performance of the PBM and subsequently affect the predictive capabilities of the BOAT approach for surface roughness estimation.

The hyperparameters are totally determined by the Bayesian optimization algorithm with the assessment index of Mean Square Error (MSE). To prove the effectiveness of the Bayesian optimization algorithm for the configuration of various hyperparameters, five groups of exemplary Hyperparameter Combinations (HC) are also presented, considering the difficulties of presenting all the combinations. The specific items of various hyperparameters for PBM and the corresponding values, as well as the hyperparameters searching space for the Bayesian optimization algorithm, are all enumerated in **Table 6**.

Table 6

Hyperparameters for the PBM comparison in the source domain.

Items	Params. scope	Optimized HC	HC#1	HC#2	HC#3	HC#4	HC#5
Filter number	(16, 32)	64	8	16	20	32	50
Dropout 1	(0.2, 0.5)	0.35	0.20	0.26	0.30	0.30	0.35
Dropout 2	(0.2, 0.5)	0.28	0.25	0.28	0.32	0.32	0.28
Dropout 3	(0.2, 0.5)	0.30	0.28	0.33	0.35	0.38	0.30
Learning rate	(10^{-4}, 10^{-3})	8×10^{-4}	10^{-3}	5×10^{-4}	2×10^{-4}	10^{-4}	10^{-3}
Decay	(10^{-6}, 10^{-4})	2.0×10^{-5}	10^{-4}	5.8×10^{-5}	6.2×10^{-5}	6.0×10^{-5}	5.0×10^{-5}
Batch size 1	(32, 256)	256	16	32	64	128	256
Batch size 2	(32, 256)	128	8	16	32	64	128
Epochs	(100, 500)	180	100	150	200	300	240

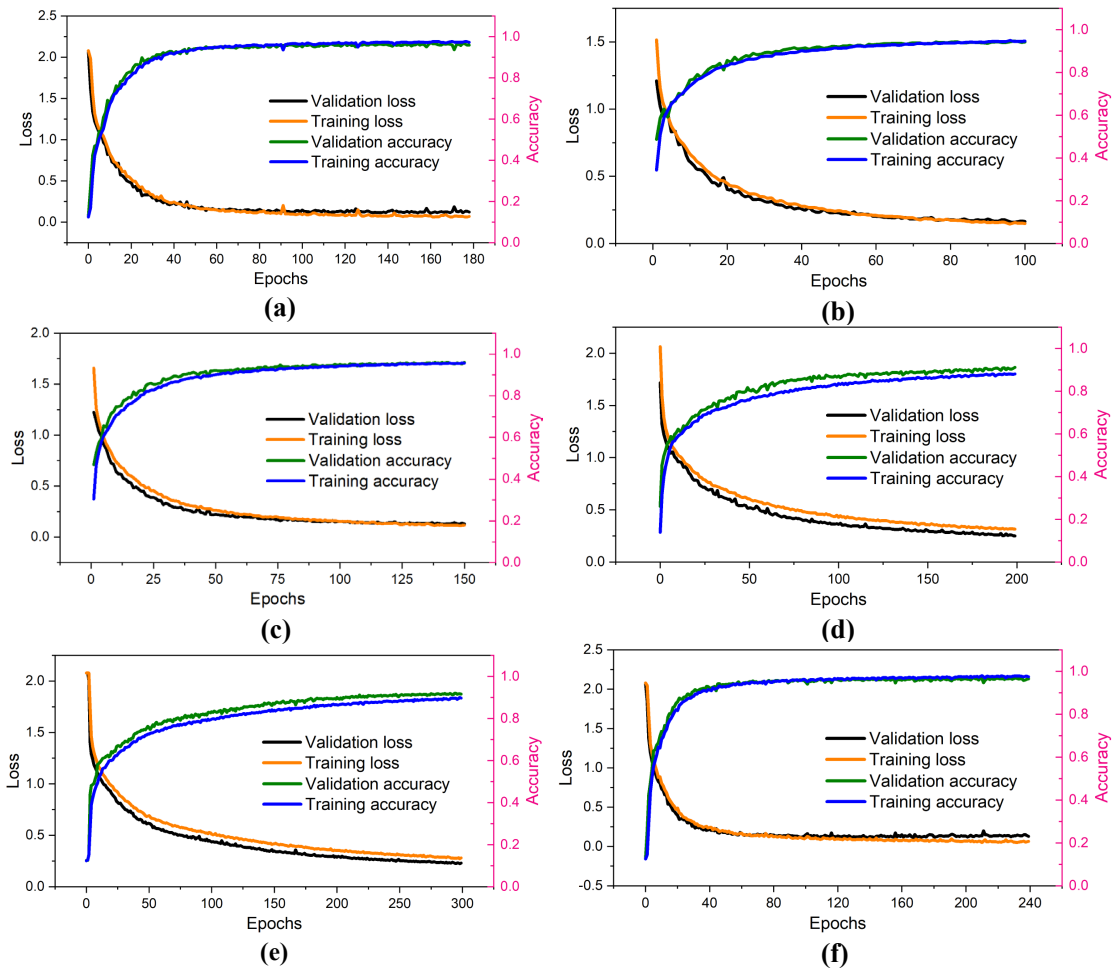

Fig. 12. Training history plots of PBM using exemplary hyperparameter combinations: (a) optimized HC, (b) HC#1, (c) HC#2, (d) HC#3, (e) HC#4, (f) HC#5.

The hyperparameters presented in **Table 6** bring six different architectures of PBM, and each PBM architecture has a distinct correlation with varying performance outcomes. All the PBM architectures enumerated in **Table 6** have undergone comprehensive training and testing, with their respective training histories visualized and depicted in **Fig. 12**. Upon analyzing this figure, it becomes apparent that the diverse architectures exhibit distinct training histories. The performance of the trained models aligns with the patterns observed in the corresponding training history plots. For

instance, both the PBM shown in **Fig. 12** (a) and (f) are sufficiently trained with good indicators of accuracy and loss, while the PBM presented in **Fig. 12** (b) and (c) are underfitting; the PBM related to **Fig. 12** (d) and (e) has a noticeable discrepancy between the training and validation curves.

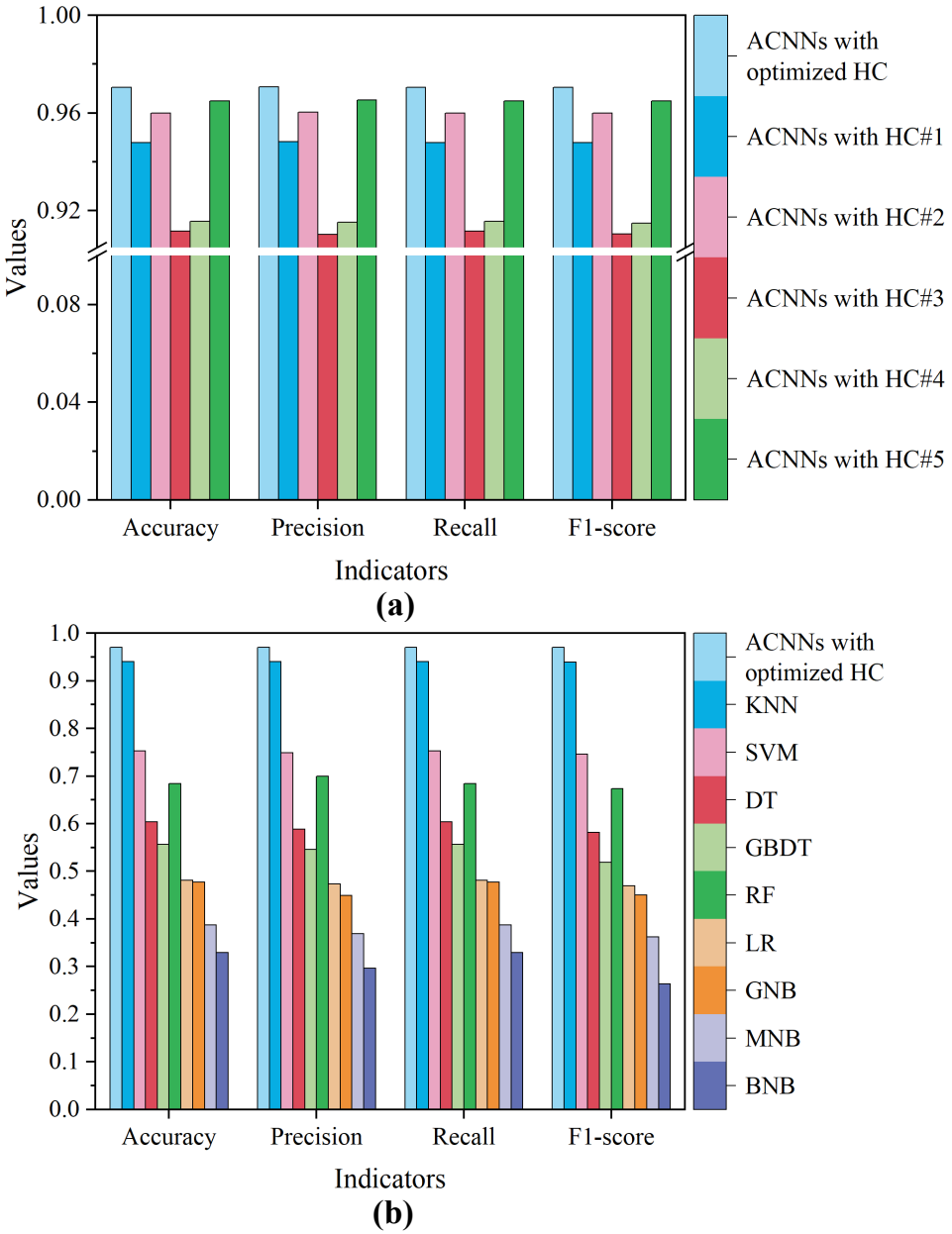

Fig. 13. Bar graph for comparison: (a) ACNNs with different hyperparameters, (b) optimized ACNNs and exemplary ML methods.

To explore the performance of the PBM with the optimized combination of the hyperparameters on the dataset consisting of FDM-printed samples in a more extensive way, PBM architectures mentioned in **Table 6** are evaluated by the four widely-accepted indicators, Accuracy, Precision, Recall, and F1-score in the ML community. To compare the performance of the PBM architectures intuitively, two bar graphs are diagramed in **Fig. 13** in terms of the above-mentioned four indicators. In **Fig. 13**, the horizontal axis represents indicators, and the vertical axis represents values. **Fig. 13** (a) is a comparative figure among PBM architectures using different hyperparameters, and the height of the bar denotes the magnitude of indicators. From **Fig. 13** (a), it can be observed that the ACNNs with the optimized hyperparameters show the maximum height, which means that this PBM has the best performance on the dataset consisting of the FDM-printed samples. The PBM with the best performance is then compared with the conventional ML methods, as shown in **Fig. 13** (b). Similarly, the height of the bars represents the magnitude of the indicators. **Fig. 13** (b) indicates that the ACNNs model with the optimized hyperparameters outperforms the exemplary ML methods, such as K-Near Neighbors (KNN), Support Vector Machine (SVM), DT, Gradient Boosting Decision Trees (GBDT), Random Forrests (RF), Linear Regression (LR), Gaussian/Multinomial/Bernoulli Naïve Bayes (GNB/MNB/BNB) classifiers, by comparison of the above-mentioned four indicator values on the same dataset.

Besides, to evaluate the performance of the PBM with the diverse hyperparameters, the corresponding diagram of the normalized CM is plotted, as shown in **Fig. 14**. It can

be seen from **Fig. 14** that the dataset consisting of FDM-printed samples is categorized into eight classes in terms of the magnitude of surface roughness. The number in each cell on the diagonal represents the proportion of correctly classified samples to the total number of samples in each category. By comparison among **Fig. 14** (a)-(f), **Fig. 14** (a) presents the maximum accuracy in predicting the surface roughness of the FDM-printed samples of the testing dataset.

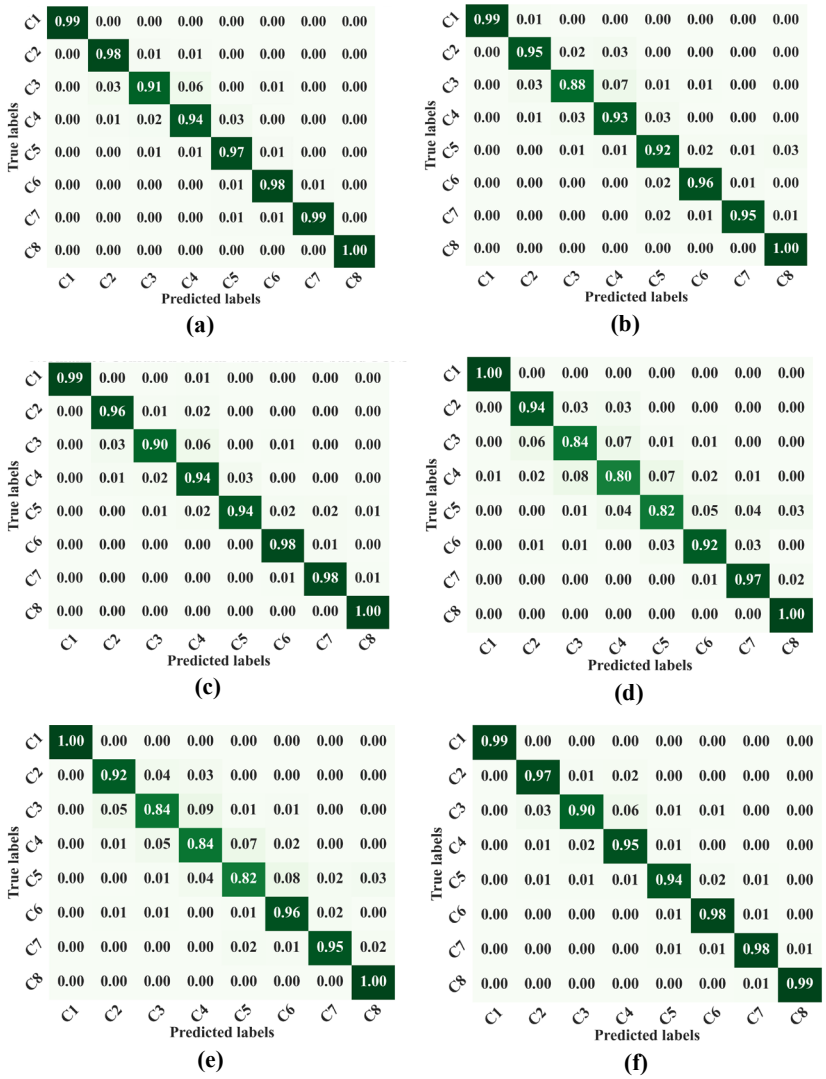

Fig. 14. Surface roughness prediction of ACNNs using different hyperparameters: (a) optimal hyperparameters, (b) HC#1, (c) HC#2, (d) HC#3, (e) HC#4, (f) HC#5.

Therefore, we can deduce that the different hyperparameters significantly affect the model performance, according to **Fig. 12** - **Fig. 14**. The model hyperparameters optimization and searching for the best PBM with the maximum performance is dramatically important before employing the BOAT approach in a new scenario. The PBM trained by the dataset from FDM-printed samples with the optimized hyperparameters is then transferred to the new application scenarios, including a small dataset to implement the objective tasks.

4.3. Performance analysis of the BOAT approach in the target domain

The ACNNs with the optimized combination of the hyperparameters serve as the PBM for the BOAT approach in the new scenarios. The BOAT approach aims to enhance performance and efficiency using the small dataset relevant to the case of SLM printing in this study. The weight matrix is learned from the dataset in the source domain and reused in the target domain with the TL strategy based on fine-tuning. The integrated Bayesian optimization into the BOAT approach automatically determined optimal hyperparameters used for retraining have been enumerated in **Table 7**.

Table 7

PBM-facilitated BOAT approach retraining with optimized hyperparameters.

	Learning rate	Decay	Batch size 1	Batch size 2	Epochs
Params. space	(0.001, 0.01)	(10^{-5}, 10^{-4})	(4, 32)	(4, 32)	(30, 180)
Optimal params.	0.0028	8.5×10^{-5}	5	32	120

The retraining of partial layers of the BOAT approach is conducted with the dataset in the target domain. This retraining process takes only 23.8 seconds on the workstation, configuring a 5950X processor, a 4070Ti graphic card, and 64GB memory in total. The plots of the training process are illustrated in **Fig. 15** with a double-Y axises graph. This figure shows that the two training loss curves present a similar trend with the epochs increasing, indicating that the BOAT approach prediction on the dataset in the target domain has low-level errors. Similarly, the training and validation accuracy curves have a prominent consistency, exhibiting superb accuracy.

In order to demonstrate the effectiveness of the BOAT approach for the surface quality prediction of the SLM-printed samples, the BOAT approach is also evaluated by the four indicators mentioned above. A bar graph is plotted to intuitively make a comparison between the BOAT approach and other conventional ML methods, as illustrated in **Fig. 16**. As already presented in **Table 4**, the dataset in the source domain and target domain has different attributes. But according to this graph, the proposed BOAT approach produces noticeably better outcomes than other conventional ML methods despite the BOAT being employed in the new case. Therefore, the results presented in **Fig. 16** convincingly demonstrate the effectiveness and the generalization capability of the proposed BOAT approach by reusing the former data from similar cases to a new scenario to implement the new tasks.

Moreover, to further effectively showcase the precision of surface roughness predictions achieved through the proposed BOAT approach in a visualized way, a

normalized CM plot has been included in **Fig. 17**. According to this figure, the numerical values present in each cell along the diagonal of the table serve as indicators of the proportion of accurately classified samples relative to the total number of samples within individual categories. These numbers hold significant importance in assessing and evaluating the classification model under scrutiny. By meticulously examining these proportions, one can ascertain valuable insights into the efficacy and precision demonstrated by the classifier, thereby obtaining a comprehensive understanding of its ability to categorize diverse samples proficiently.

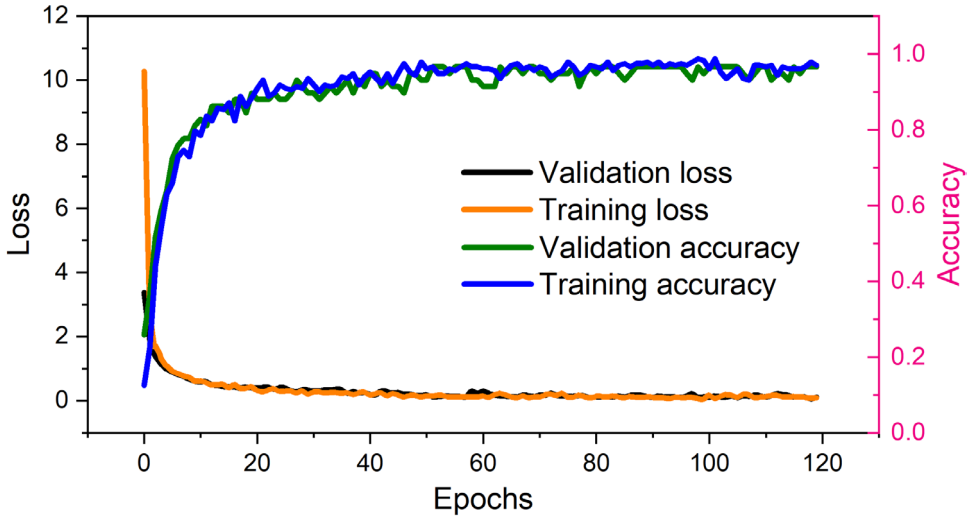

Fig. 15. Training history plots of the BOAT on the small dataset composed of the SLM-printed Ti6Al4V samples in the target domain.

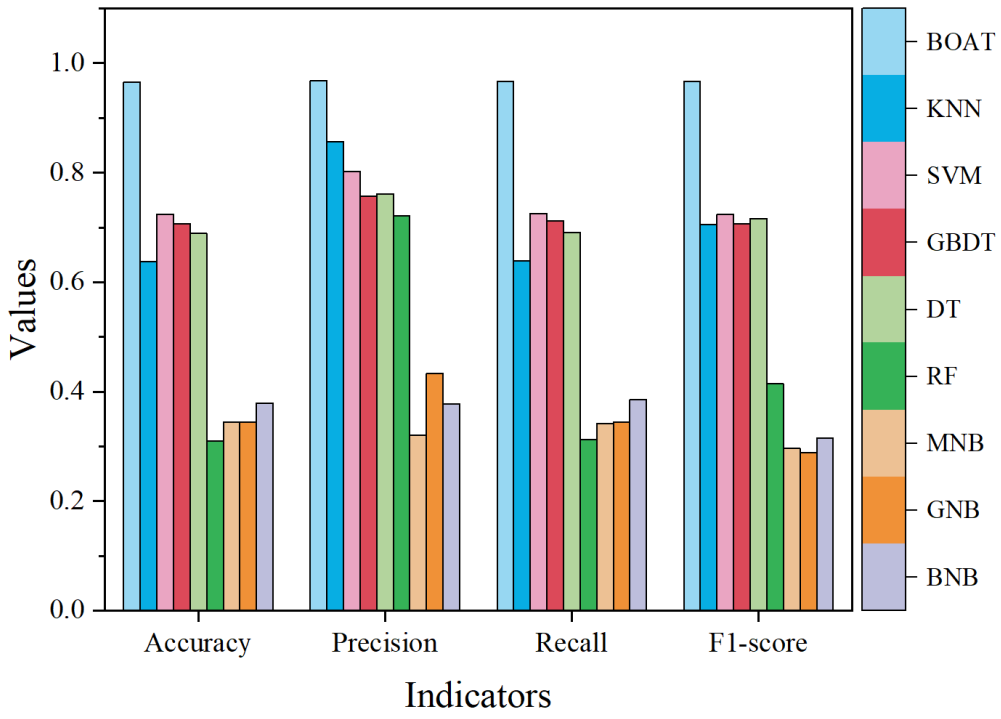

Fig. 16. Comparison between BOAT and the exemplary ML methods.

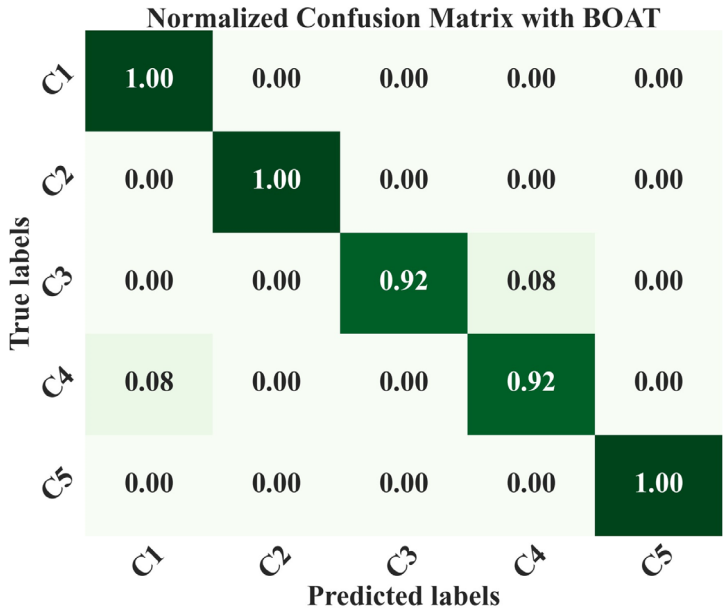

Fig. 17. Normalized CM of BOAT prediction on the small dataset composed of the SLM-printed Ti6Al4V samples in the target domain.

5. Conclusions

This study explores the critical aspect of the SLM-based 3D printing quality using Ti6Al4V alloy powder. In pursuit of this objective, we proposed an innovative framework integrating a Bayesian optimization algorithm with an attention mechanism-enhanced transfer learning methodology named the BOAT approach.

The results obtained from the experiments in the source and target domains for validation underscore the perspective of the BOAT approach in manipulating printing parameters to achieve improved printing quality for the SLM process using Ti6Al4V alloy powders. The optimal performance of the PBM is achieved by hyperparameters optimization and detailed analyses by plotting training history, visualizing performance indicator values, and normalized CM diagrams. By deploying the proposed BOAT framework, we also promote the capability to predict printing quality. The proposed BOAT approach facilitates accurate quality estimation in the new scenarios by leveraging insights from prior FDM 3D printing processes and incorporating attention mechanisms. This methodology effectively mitigated challenges associated with limited labeled data, offering valuable implications for quality prediction within Ti6Al4V alloy 3D printing.

The findings of this study contribute to the advancement of 3D printing by providing potential strategies for manipulating and predicting printing quality, specifically within the context of Ti6Al4V alloy prints. Future research endeavors may expand upon this work by exploring different alloys or developing more efficient,

automatic, and intelligent model frameworks. Ultimately, these advancements will foster wider adoption of 3D printing technologies across various industrial sectors.

Acknowledgement

Assoc. Prof. Dr. Jianjian Zhu would like to give thanks for the support from the Young Scientists Fund of the National Natural Science Foundation of China (Grant No. 52205171).

CRediT authorship contribution statement

Jianjian Zhu: Conceptualization, Data curation, Formal analysis, Investigation, Methodology, Software, Funding acquisition, Writing – original draft, Writing – review & editing. **Zhongqing Su:** Methodology, Supervision. **Qingqing Wang:** Investigation, Validation. **Runze Hao:** Investigation. **Zifeng Lan:** Writing – review & editing. **Frankie Siu-fai Chan:** Investigation. **Jiaqiang Li:** Supervision. **Sidney Wing-fai Wong:** Project administration.

Declaration of Competing Interest

The authors declare that they have no known competing financial interests or personal relationships that could have appeared to influence the work reported in this paper.

References

[1] D.Yu. Pimenov, L.F. Berti, G. Pintaude, G.X. Peres, Y. Chaurasia, N. Khanna, K. Giasin, Influence of selective laser melting process parameters on the surface integrity of difficult-to-cut alloys: comprehensive review and future prospects, Int. J. Adv. Manuf. Technol. 127 (2023) 1071–1102. https://doi.org/10.1007/s00170-023-11541-8.

[2] H.M. Khan, Y. Karabulut, O. Kitay, Y. Kaynak, I.S. Jawahir, Influence of the post-processing operations on surface integrity of metal components produced by laser powder bed fusion additive manufacturing: a review, Mach. Sci. Technol. 25 (2020) 118–176. https://doi.org/10.1080/10910344.2020.1855649.

[3] S. Sendino, S. Martinez, F. Lartategui, M. Gardon, A. Lamikiz, J.J. Gonzalez, Effect of powder particle size distribution on the surface finish of components manufactured by laser powder bed fusion, Int. J. Adv. Manuf. Technol. 124 (2023) 789–799. https://doi.org/10.1007/s00170-022-10423-9.

[4] K. Riener, N. Albrecht, S. Ziegelmeier, R. Ramakrishnan, L. Haferkamp, A.B. Spierings, G.J. Leichtfried, Influence of particle size distribution and morphology on the properties of the powder feedstock as well as of AlSi10Mg parts produced by laser powder bed fusion (LPBF), Addit. Manuf. 34 (2020) 101286. https://doi.org/10.1016/j.addma.2020.101286.

[5] H. Miao, F. Yusof, M.S.A. Karim, I.A. Badruddin, M. Hussien, S. Kamangar, H. Zhang, Process Parameters Optimization for Selective Laser Melting of Alsi10mg-316l Multi-Material Parts Using Machine Learning Approach, (2023).

https://doi.org/10.2139/ssrn.4365803.

[6] Y. Jing, P. Wang, X. Yan, Effect of Process Parameters and Layer Thickness on the Quality and Performance of Ti-6Al-4V Fabricated by Selective Laser Melting, Coatings. 11 (2021) 1323. https://doi.org/10.3390/coatings11111323.

[7] B. Song, S. Dong, B. Zhang, H. Liao, C. Coddet, Effects of processing parameters on microstructure and mechanical property of selective laser melted Ti6Al4V, Mater. Des. 35 (2012) 120–125. https://doi.org/10.1016/j.matdes.2011.09.051.

[8] A. Charles, A. Elkaseer, L. Thijs, V. Hagenmeyer, S. Scholz, Effect of Process Parameters on the Generated Surface Roughness of Down-Facing Surfaces in Selective Laser Melting, Appl. Sci. 9 (2019) 1256. https://doi.org/10.3390/app9061256.

[9] A.H. Maamoun, Y.F. Xue, M.A. Elbestawi, S.C. Veldhuis, Effect of Selective Laser Melting Process Parameters on the Quality of Al Alloy Parts: Powder Characterization, Density, Surface Roughness, and Dimensional Accuracy, Materials. 11 (2018) 2343. https://doi.org/10.3390/ma11122343.

[10] D. Wang, J. Lv, X. Wei, D. Lu, C. Chen, Study on Surface Roughness Improvement of Selective Laser Melted Ti6Al4V Alloy, Crystals. 13 (2023) 306. https://doi.org/10.3390/cryst13020306.

[11] Z. Zheng, X. Jin, Y. Bai, Y. Yang, C. Ni, W.F. Lu, H. Wang, Microstructure and anisotropic mechanical properties of selective laser melted Ti6Al4V alloy under different scanning strategies, Mater. Sci. Eng. A. 831 (2022) 142236. https://doi.org/10.1016/j.msea.2021.142236.

[12] A.M. Khorasani, I. Gibson, A.R. Ghaderi, Rheological characterization of process parameters influence on surface quality of Ti-6Al-4V parts manufactured by selective laser melting, Int. J. Adv. Manuf. Technol. 97 (2018) 3761–3775. https://doi.org/10.1007/s00170-018-2168-6.

[13] R. Sheshadri, M. Nagaraj, A. Lakshmikanthan, M.P.G. Chandrashekarappa, D.Y. Pimenov, K. Giasin, R.V.S. Prasad, S. Wojciechowski, Experimental investigation of selective laser melting parameters for higher surface quality and microhardness properties: taguchi and super ranking concept approaches, J. Mater. Res. Technol. 14 (2021) 2586–2600. https://doi.org/10.1016/j.jmrt.2021.07.144.

[14] D.N. Aqilah, A.K.M. Sayuti, Y. Farazila, D.Y. Suleiman, M.A.N. Amirah, W.B.W.N. Izzati, Effects of Process Parameters on the Surface Roughness of Stainless Steel 316L Parts Produced by Selective Laser Melting, J. Test. Eval. 46 (2018) 1673–1683. https://doi.org/10.1520/JTE20170140.

[15] M. Oyesola, K. Mpofu, N. Mathe, S. Fatoba, S. Hoosain, I. Daniyan, Optimization of selective laser melting process parameters for surface quality performance of the fabricated Ti6Al4V, Int. J. Adv. Manuf. Technol. 114 (2021) 1585–1599. https://doi.org/10.1007/s00170-021-06953-3.

[16] Z. Li, I. Kucukkoc, D.Z. Zhang, F. Liu, Optimising the process parameters of selective laser melting for the fabrication of Ti6Al4V alloy, Rapid Prototyp. J. 24 (2018) 150–159. https://doi.org/10.1108/RPJ-03-2016-0045.

[17] N.A. Fountas, J.D. Kechagias, N.M. Vaxevanidis, Optimization of Selective Laser

Sintering/Melting Operations by Using a Virus-Evolutionary Genetic Algorithm, Machines. 11 (2023) 95. https://doi.org/10.3390/machines11010095.

[18] Q. Xia, J. Han, A Multi-Objectives Genetic Algorithm Based Predictive Model and Strategy Optimization during SLM Process, Materials. 15 (2022) 4607. https://doi.org/10.3390/ma15134607.

[19] V. Maitra, J. Shi, C. Lu, Robust prediction and validation of as-built density of Ti-6Al-4V parts manufactured via selective laser melting using a machine learning approach, J. Manuf. Process. 78 (2022) 183–201. https://doi.org/10.1016/j.jmapro.2022.04.020.

[20] P. Shubham, A. Sharma, P.N. Vishwakarma, R.K. Phanden, Predicting Strength of Selective Laser Melting 3D Printed A1Si10Mg Alloy Parts by Machine Learning Models, in: 2021 8th Int. Conf. Signal Process. Integr. Netw. SPIN, 2021: pp. 745–749. https://doi.org/10.1109/SPIN52536.2021.9566142.

[21] S. Chaudhry, A. Soulaïmani, A Comparative Study of Machine Learning Methods for Computational Modeling of the Selective Laser Melting Additive Manufacturing Process, Appl. Sci. 12 (2022) 2324. https://doi.org/10.3390/app12052324.

[22] C. Barile, C. Casavola, G. Pappalettera, V.P. Kannan, D.K. Mpoyi, Acoustic Emission and Deep Learning for the Classification of the Mechanical Behavior of AlSi10Mg AM-SLM Specimens, Appl. Sci. 13 (2023) 189. https://doi.org/10.3390/app13010189.

[23] K.L. Raju, S. Thapliyal, S. Sigatapu, A.K. Shukla, G. Bajargan, B. Pant, Process

Parameter Dependent Machine Learning Model for Densification Prediction of Selective Laser Melted Al-50Si Alloy and its Validation, J. Mater. Eng. Perform. 31 (2022) 8451–8458. https://doi.org/10.1007/s11665-022-06831-3.

[24] S. Miyazaki, M. Kusano, D.S. Bulgarevich, S. Kishimoto, A. Yumoto, M. Watanabe, Image Segmentation and Analysis for Microstructure and Property Evaluations on Ti–6Al–4V Fabricated by Selective Laser Melting, Mater. Trans. 60 (2019) 561–568. https://doi.org/10.2320/matertrans.MBW201806.

[25] H.S. Park, D.S. Nguyen, T. Le-Hong, X. Van Tran, Machine learning-based optimization of process parameters in selective laser melting for biomedical applications, J. Intell. Manuf. 33 (2022) 1843–1858. https://doi.org/10.1007/s10845-021-01773-4.

[26] A. Aditya Sharma, U. Mohammed, H. Goutham, S. Sagar, Y. Sharath Kumar, Y. Chethan, Surface Fault Detection in 3D Printed Objects Using Deep Learning, Int. J. Res. Appl. Sci. Eng. Technol. 10 (2022) 4258–4267. https://doi.org/10.22214/ijraset.2022.45820.

[27] S.A. Shevchik, C. Kenel, C. Leinenbach, K. Wasmer, Acoustic emission for in situ quality monitoring in additive manufacturing using spectral convolutional neural networks, Addit. Manuf. 21 (2018) 598–604. https://doi.org/10.1016/j.addma.2017.11.012.

[28] B. Rankouhi, S. Jahani, F.E. Pfefferkorn, D.J. Thoma, Compositional grading of a 316L-Cu multi-material part using machine learning for the determination of selective

laser melting process parameters, Addit. Manuf. 38 (2021) 101836. https://doi.org/10.1016/j.addma.2021.101836.

[29] N. Burkart, M.F. Huber, A Survey on the Explainability of Supervised Machine Learning, J. Artif. Intell. Res. 70 (2021) 245–317. https://doi.org/10.1613/jair.1.12228.

[30] D.S. Nguyen, H.S. Park, C.M. Lee, Optimization of selective laser melting process parameters for Ti-6Al-4V alloy manufacturing using deep learning, J. Manuf. Process. 55 (2020) 230–235. https://doi.org/10.1016/j.jmapro.2020.04.014.

[31] Y. Chen, H. Wang, Y. Wu, H. Wang, Predicting the Printability in Selective Laser Melting with a Supervised Machine Learning Method, Materials. 13 (2020) 5063. https://doi.org/10.3390/ma13225063.

[32] H. Bao, S. Wu, Z. Wu, G. Kang, X. Peng, P.J. Withers, A machine-learning fatigue life prediction approach of additively manufactured metals, Eng. Fract. Mech. 242 (2021) 107508. https://doi.org/10.1016/j.engfracmech.2020.107508.

[33] I. La Fé-Perdomo, J. Ramos-Grez, R. Mujica, M. Rivas, Surface roughness Ra prediction in Selective Laser Melting of 316L stainless steel by means of artificial intelligence inference, J. King Saud Univ. - Eng. Sci. 35 (2023) 148–156. https://doi.org/10.1016/j.jksues.2021.03.002.

[34] M. Zhang, C.-N. Sun, X. Zhang, P.C. Goh, J. Wei, D. Hardacre, H. Li, High cycle fatigue life prediction of laser additive manufactured stainless steel: A machine learning approach, Int. J. Fatigue. 128 (2019) 105194. https://doi.org/10.1016/j.ijfatigue.2019.105194.

[35] W. Ren, J. Mazumder, In-situ porosity recognition for laser additive manufacturing of 7075-Al alloy using plasma emission spectroscopy, Sci. Rep. 10 (2020) 19493. https://doi.org/10.1038/s41598-020-75131-4.

[36] N.H. Paulson, B. Gould, S.J. Wolff, M. Stan, A.C. Greco, Correlations between thermal history and keyhole porosity in laser powder bed fusion, Addit. Manuf. 34 (2020) 101213. https://doi.org/10.1016/j.addma.2020.101213.

[37] G.O. Barrionuevo, J.A. Ramos-Grez, M. Walczak, C.A. Betancourt, Comparative evaluation of supervised machine learning algorithms in the prediction of the relative density of 316L stainless steel fabricated by selective laser melting, Int. J. Adv. Manuf. Technol. 113 (2021) 419–433. https://doi.org/10.1007/s00170-021-06596-4.

[38] I. La Fé-Perdomo, J.A. Ramos-Grez, I. Jeria, C. Guerra, G.O. Barrionuevo, Comparative analysis and experimental validation of statistical and machine learning-based regressors for modeling the surface roughness and mechanical properties of 316L stainless steel specimens produced by selective laser melting, J. Manuf. Process. 80 (2022) 666–682. https://doi.org/10.1016/j.jmapro.2022.06.021.

[39] J. Li, Z. Yang, G. Qian, F. Berto, Machine learning based very-high-cycle fatigue life prediction of Ti-6Al-4V alloy fabricated by selective laser melting, Int. J. Fatigue. 158 (2022) 106764. https://doi.org/10.1016/j.ijfatigue.2022.106764.

[40] Z. Yang, M. Yang, R. Sisson, Y. Li, J. Liang, Machine learning model to predict tensile properties of annealed Ti6Al4V parts prepared by selective laser melting, AI EDAM. 36 (2022) e30. https://doi.org/10.1017/S0890060422000117.

[41] Y. Tang, M. Rahmani Dehaghani, G.G. Wang, Review of transfer learning in modeling additive manufacturing processes, Addit. Manuf. 61 (2023) 103357. https://doi.org/10.1016/j.addma.2022.103357.

[42] E. Westphal, H. Seitz, A machine learning method for defect detection and visualization in selective laser sintering based on convolutional neural networks, Addit. Manuf. 41 (2021) 101965. https://doi.org/10.1016/j.addma.2021.101965.

[43] F.G. Fischer, M.G. Zimmermann, N. Praetzsch, C. Knaak, Monitoring of the powder bed quality in metal additive manufacturing using deep transfer learning, Mater. Des. 222 (2022) 111029. https://doi.org/10.1016/j.matdes.2022.111029.

[44] H. Kim, H. Lee, S.-H. Ahn, Systematic deep transfer learning method based on a small image dataset for spaghetti-shape defect monitoring of fused deposition modeling, J. Manuf. Syst. 65 (2022) 439–451. https://doi.org/10.1016/j.jmsy.2022.10.009.

[45] D.A.J. Brion, M. Shen, S.W. Pattinson, Automated recognition and correction of warp deformation in extrusion additive manufacturing, Addit. Manuf. 56 (2022) 102838. https://doi.org/10.1016/j.addma.2022.102838.

[46] M. Mehta, C. Shao, Federated learning-based semantic segmentation for pixel-wise defect detection in additive manufacturing, J. Manuf. Syst. 64 (2022) 197–210. https://doi.org/10.1016/j.jmsy.2022.06.010.

[47] P. Pandita, S. Ghosh, V.K. Gupta, A. Meshkov, L. Wang, Application of Deep Transfer Learning and Uncertainty Quantification for Process Identification in Powder Bed Fusion, ASCE-ASME J Risk Uncert Engrg Sys Part B Mech Engrg. 8 (2021).

https://doi.org/10.1115/1.4051748.

[48] V. Pandiyan, R. Drissi-Daoudi, S. Shevchik, G. Masinelli, T. Le-Quang, R. Logé, K. Wasmer, Deep transfer learning of additive manufacturing mechanisms across materials in metal-based laser powder bed fusion process, J. Mater. Process. Technol. 303 (2022) 117531. https://doi.org/10.1016/j.jmatprotec.2022.117531.

[49] J. Francis, A. Sabbaghi, M. Ravi Shankar, M. Ghasri-Khouzani, L. Bian, Efficient Distortion Prediction of Additively Manufactured Parts Using Bayesian Model Transfer Between Material Systems, J. Manuf. Sci. Eng. 142 (2020). https://doi.org/10.1115/1.4046408.

[50] S. Liu, A.P. Stebner, B.B. Kappes, X. Zhang, Machine learning for knowledge transfer across multiple metals additive manufacturing printers, Addit. Manuf. 39 (2021) 101877. https://doi.org/10.1016/j.addma.2021.101877.

[51] J. Ren, A.-T. Wei, Z. Jiang, H. Wang, X. Wang, Improved Modeling of Kinematics-Induced Geometric Variations in Extrusion-Based Additive Manufacturing Through Between-Printer Transfer Learning, IEEE Trans. Autom. Sci. Eng. 19 (2022) 2310–2321. https://doi.org/10.1109/TASE.2021.3063389.

[52] L. Cheng, K. Wang, F. Tsung, A hybrid transfer learning framework for in-plane freeform shape accuracy control in additive manufacturing, IISE Trans. 53 (2020) 298–312. https://doi.org/10.1080/24725854.2020.1741741.

[53] L. Cheng, F. Tsung, A. Wang, A Statistical Transfer Learning Perspective for Modeling Shape Deviations in Additive Manufacturing, IEEE Robot. Autom. Lett. 2

(2017) 1988–1993. https://doi.org/10.1109/LRA.2017.2713238.

[54] C.Y. Yap, C.K. Chua, Z.L. Dong, Z.H. Liu, D.Q. Zhang, L.E. Loh, S.L. Sing, Review of selective laser melting: Materials and applications, Appl. Phys. Rev. 2 (2015) 041101. https://doi.org/10.1063/1.4935926.

[55] J. Lv, K. Luo, H. Lu, Z. Wang, J. Liu, J. Lu, Achieving high strength and ductility in selective laser melting Ti-6Al-4V alloy by laser shock peening, J. Alloys Compd. 899 (2022) 163335. https://doi.org/10.1016/j.jallcom.2021.163335.

[56] B. Nagarajan, Z. Hu, X. Song, W. Zhai, J. Wei, Development of Micro Selective Laser Melting: The State of the Art and Future Perspectives, Engineering. 5 (2019) 702–720. https://doi.org/10.1016/j.eng.2019.07.002.

[57] Z. Jiao, X. Wu, H. Yu, R. Xu, L. Wu, High cycle fatigue behavior of a selective laser melted Ti6Al4V alloy: Anisotropy, defects effect and life prediction, Int. J. Fatigue. 167 (2023) 107252. https://doi.org/10.1016/j.ijfatigue.2022.107252.

[58] J. Li, H. Wu, H. Liu, D. Zuo, Surface and property characterization of selective laser-melted Ti-6Al-4V alloy after laser polishing, Int. J. Adv. Manuf. Technol. (2023). https://doi.org/10.1007/s00170-023-11880-6.

[59] S. Önder, N. Saklakoğlu, A. Sever, Selective laser melting of Ti6Al4V alloy: Effect of post-processing on fatigue life, residual stress, microstructure, microhardness and surface roughness, Mater. Charact. 196 (2023) 112571. https://doi.org/10.1016/j.matchar.2022.112571.

[60] J. Airao, H. Kishore, C.K. Nirala, Comparative analysis of tool wear in micro-

milling of wrought and selective laser melted Ti6Al4V, Wear. 523 (2023) 204788. https://doi.org/10.1016/j.wear.2023.204788.

[61] Z. Niu, G. Zhong, H. Yu, A review on the attention mechanism of deep learning, Neurocomputing. 452 (2021) 48–62. https://doi.org/10.1016/j.neucom.2021.03.091.

[62] M.-H. Guo, T.-X. Xu, J.-J. Liu, Z.-N. Liu, P.-T. Jiang, T.-J. Mu, S.-H. Zhang, R.R. Martin, M.-M. Cheng, S.-M. Hu, Attention mechanisms in computer vision: A survey, Comput. Vis. Media. 8 (2022) 331–368. https://doi.org/10.1007/s41095-022-0271-y.

[63] S.J. Pan, Q. Yang, A Survey on Transfer Learning, IEEE Trans. Knowl. Data Eng. 22 (2010) 1345–1359. https://doi.org/10.1109/TKDE.2009.191.

[64] C. Tan, F. Sun, T. Kong, W. Zhang, C. Yang, C. Liu, A Survey on Deep Transfer Learning, in: V. Kůrková, Y. Manolopoulos, B. Hammer, L. Iliadis, I. Maglogiannis (Eds.), Artif. Neural Netw. Mach. Learn. – ICANN 2018, Springer International Publishing, Cham, 2018: pp. 270–279. https://doi.org/10.1007/978-3-030-01424-7_27.

[65] K. Weiss, T.M. Khoshgoftaar, D. Wang, A survey of transfer learning, J. Big Data. 3 (2016) 9. https://doi.org/10.1186/s40537-016-0043-6.